Sodium vapor cell laser guide star experiments for continuous wave model validation

Felipe Pedreros Bustos[a], Ronald Holzlöhner[b], Dmitry Budker[a], Steffan Lewis[b], and Simon Rochester[c]

[a]Johannes Gutenberg Universität, Staudingerweg 7, 55128 Mainz, Germany
[b]European Southern Observatory, Karl-Schwarzschild-Str. 2, D-85748 Garching b. Muenchen, Germany
[c]Rochester Scientific, LLC, El Cerrito, CA.

ABSTRACT

Recent numerical simulations and experiments on sodium Laser Guide Star (LGS) have shown that a continuous wave (CW) laser with circular polarization and re-pumping should maximize the fluorescent photon return flux to the wavefront sensor for adaptive optics applications. The orientation and strength of the geomagnetic field in the sodium layer also play an important role affecting the LGS return flux. Field measurements of the LGS return flux show agreement with the CW LGS model, however, fluctuations in the sodium column abundance and geomagnetic field intensity, as well as atmospheric turbulence, induce experimental uncertainties. We describe a laboratory experiment to measure the photon return flux from a sodium vapor cell illuminated with a 589 nm CW laser beam, designed to approximately emulate a LGS under controlled conditions. Return flux measurements are carried out controlling polarization, power density, re-pumping, laser linewidth, and magnetic field intensity and orientation. Comparison with the numerical CW simulation package Atomic Density Matrix are presented and discussed.

Keywords: Laser Guide Star, sodium vapor cell, return flux

1. INTRODUCTION

Artificial sodium laser guide stars (LGS) are used as a reference for atmospheric-turbulence compensation adaptive optics systems. Since the first reported demonstration of this technique in 1987,[1] there have been significant efforts to maximize the brightness of a sodium LGS in order to increase the signal-to-noise ratio of the wavefront sensing. Therefore, several groups have developed new types of lasers and investigated the atomic interaction of sodium with a resonant laser beam. Testing of different laser formats is usually carried out in the field to directly measure the photon return from the LGS in the mesosphere.[2] An alternative to field tests is to perform laboratory-environment experiments using sodium vapor cells.[3, 4] Atomic conditions in a vapor cell are different from the ones found typically in the mesosphere, although a correct understanding of the physical processes involved in a confined volume allows us to compare it with the behavior of a LGS in the mesosphere. A laboratory LGS test bench enables us to use it as a flexible platform for testing any LGS format under controlled conditions, as well as a diagnosis tool for any LGS facility.

In this paper, we report on the development of a LGS test bench based on a sodium vapor cell for the validation of a continuous wave (CW) LGS return flux optimization model.[5] This experiment complements the results from the return flux field-test campaign performed by the European Southern Observatory (ESO) at Tenerife island as reported in a related paper in these proceedings.[6]

In Section 2 we present the CW LGS return flux model and the parameters used for the vapor cell experiment. In Section 3 we describe the experimental setup and characterization of the key variables (linewidth, repumping ratio, beam size, and polarization). In Section 4 we show the results for backward fluorescence from a vapor cell and compare with simulations using the LGSBloch Atomic Density Matrix package.[7] We conclude in Section 5 and discuss the possibilities of this type of experiment.

Further author information: (Send correspondence to F.P.B.)
F.P.B.: E-mail: pedreros (at) uni-mainz.de, Telephone: +49 6131 3924605

2. MODELING

Several models have been developed to calculate the effective sodium return flux from a LGS. The fluorescence of sodium atoms under the illumination of a resonant light beam depends on the atmospheric conditions (including other constituent gases), geomagnetic field, collisions among atoms, and the interaction of the light beam with sodium. The evolution of this complex interaction can be numerically solved using Bloch equations,[8] rate equations,[9] and also methods that combine Bloch and rate equations approaches. In this paper, we follow the Bloch-equation method as presented by Holzlöhner *et al.*[10] for the optimization of a CW laser guide star. This is implemented with the LGSBloch package included in the open-source Atomic Density Matrix (ADM)[7] package for Mathematica that we use to perform the sodium return flux simulations. This method takes into account the following effects: spontaneous and stimulated emission, geomagnetic field, light polarization, recoil, about 100 coupled velocity groups including velocity-changing collisions and spin exchange, finite atomic dwell time, laser linewidth, and repumping.

In our experiment, we observe the backward fluorescence from sodium atoms, contained in vapor cell with no buffer gas, excited with a 589.1 nm CW laser beam. The environmental conditions and dynamics inside the vapor cell differ from those in the mesosphere. The key environmental parameters affecting the behavior of sodium atoms in a vapor cell are: temperature, velocity-changing collision rate and spin-exchange rate.

The mean free path ℓ of a gas at temperature T, pressure P, and particle diameter d_p is given by:[11]

$$\ell = \frac{k_B T}{\pi d_p^2 P \sqrt{2}}, \tag{1}$$

where k_B is the Boltzmann constant. We assume the diameter of the sodium atom as twice its Wan-der-Waals radius of 227 pm. For a gas cell at 383 K, the sodium vapor pressure is $P = 4.7 \cdot 10^{-5}$ Pa, giving a mean free path of 122 m.

In our vapor cell, collisions with the walls are spin-randomizing, since we are not using any spin-preserving coating. We use a vapor cell without any buffer gas, and because the dimensions of the vapor cell are much smaller than the sodium mean free path ℓ at the experiment conditions, a sodium atom will likely collide with the cell walls before a collision with another atom. We assume that every wall collision will completely reset the velocity and spin of an atom and will introduce a "fresh" sodium atom to the system. The rate for this process is characterized by the average wall-to-wall collision rate.

For a system in thermodynamic equilibrium, the Maxwell-Boltzmann velocity distribution gives the mean speed of a molecule as follows:[11]

$$\overline{v} = \sqrt{\frac{8RT}{\pi M}}, \tag{2}$$

where R is the gas constant, and M is the molar mass of sodium. For T=383 K, the average velocity of sodium atoms is 594 m/s. The average distance ℓ_w between wall-to-wall collisions in a cylindrical cell of radius R and length L is given by:[12]

$$\ell_w = 2\frac{RL}{R + L}. \tag{3}$$

For a vapor cell of 100 mm long by 23 mm internal diameter, the mean wall collision path length ℓ_w is 20.6 mm.

Therefore, the characteristic wall-to-wall collision rate for the vapor cell system is given by $\overline{v}/\ell_w = 1/(35\ \mu s)$. If we assume that the laser beam completely fills the vapor cell volume, this parameter can be seen as the beam–atom exchange rate $\gamma_{ex} = 1/(35\ \mu s)$. The estimated typical velocity-changing collision rate of sodium in the mesosphere is $\gamma_{cc}^{meso} = 1/(35\ \mu s)$. The estimated mesosphere spin-exchange rate is about $\gamma_s^{meso} = 1/(490\ \mu s)$ and the beam atom exchange rate is $\gamma_{ex}^{meso} = 1/(6.0\ ms)$.[10]

The temperature of the cell weakly affects the parameters mentioned above, and more strongly affects the vapor pressure of sodium and its atomic density. The absorption cross-section of the sodium D_2 line ($3^2S_{1/2} \rightarrow 3^2P_{3/2}$) is shown in Figure 1 for temperatures of 170 K (mesosphere) and 383 K (laboratory). The highest cross-section peak is centered at the v_0 frequency which corresponds to the $3^2S_{1/2}(F = 2) \rightarrow 3^2P_{3/2}$ transition, referred to as the D_2a transition. The second peak corresponds to the $3^2S_{1/2}(F = 1) \rightarrow 3^2P_{3/2}$ transition,

referred to as the D_2b transition, which is 1772 MHz above the D_2a frequency. Figure 1 shows that that the Doppler broadening of the sodium absorption line in the mesosphere is 1 GHz, while at 383 K the FWHM Doppler profile is 1.49 GHz, leading to a larger overlap between the D_2a and D_2b profiles.
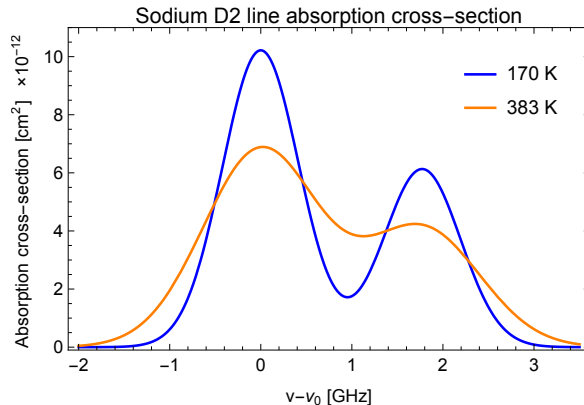

Figure 1. Sodium absorption cross-section centered at the D_2a transition for gas temperatures of 170 K (mesosphere) and 383 K (vapor cell).

3. EXPERIMENTAL SETUP

Figure 2 shows the sodium cell experiment setup. The light source consists of a narrow-band frequency-doubled Raman fiber amplifier laser, providing up to 7 W of a 589 nm single-mode continuous wave beam. An acousto-optic modulator (AOM) was used for intensity control and amplitude modulation. We have chosen to work with the first diffraction order because its extinction ratio is larger than the zero-order. A half-wave plate was placed after the AOM to align the linear polarization to the electro-optics modulator (EOM) axis. The EOM (QUBIG EO-NA23-5K) was driven with a 1.713 GHz 1W RF signal able to generate the repumping sideband with a power split ratio near 11%. The half-wave and quarter-wave plates provided polarization control of the beam. A beamsplitter picks up a fraction of the power to the monitor branch which consists of a 10 GHz free spectral range Fabry-Perot spectrum analyzer and a power meter. The beam is expanded and collimated by the L_1 and L_2 lenses.

The apodizing filter (AF, Edmund Optics #64-385 0.04-1.0 OD) attenuates the central part of the beam and flattens the intensity profile. A 2" non-polarizing pellicle beamsplitter (Thorlabs BP250 50:50) was used to reflect the backward fluorescence from the sodium vapor cell to the 2" collecting lens L_4 that focuses the fluorescence into an amplified photodiode (Thorlabs PDA100A). The cell oven was wrapped with a single layer of high-permeability magnetic shield foil, providing 10 dB of magnetic field attenuation in the transverse laser beam direction (measured with a fluxgate magnetometer). The light power incident on the cell was measured with a calibrated photodetector at the output port. The lens-photodiode assembly was swapped with a free-space polarimeter (Thorlabs PAX5710VIS-T) for measuring the polarization state of the beam. When backward fluorescence measurements were carried out, the output beam was dumped to avoid backward reflection from the optical components.

The temperature of the vapor cell oven was controlled with a DC power supply set to constant current. The temperature of the vapor cell was measured at two opposite points (top and bottom) on the surface of the cell using K-type thermocouples.
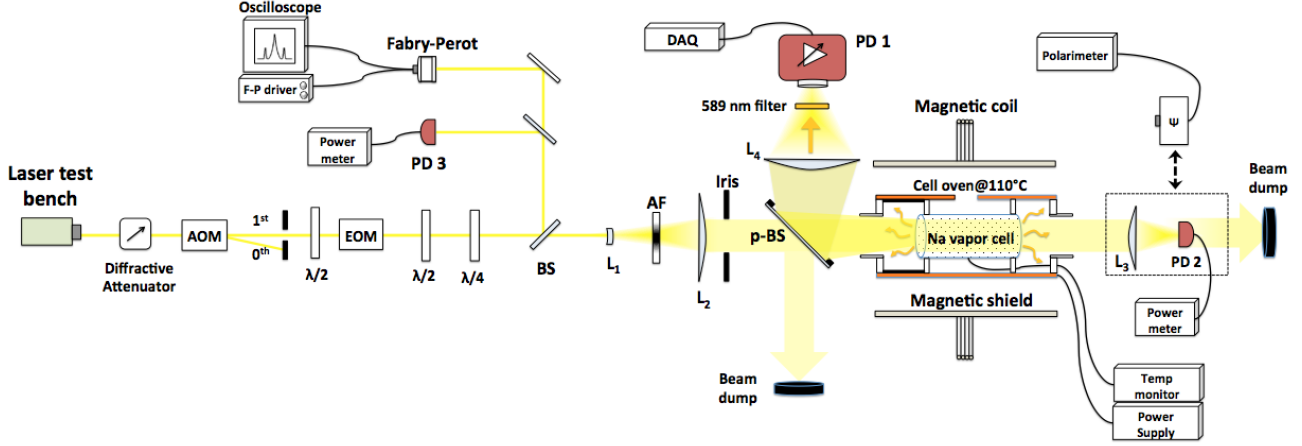
Figure 2. Setup for return flux measurements from a sodium vapor cell.

3.1 Laser linewidth

The linewidth of the laser source has been measured using a self-heterodyne scheme.[13] In a self-heterodyne scheme, a frequency shifted branch of the laser beam under test is mixed on a fast photodetector with a delayed version of the unshifted beam, producing a beat note at the offset frequency with an RF bandwidth twice the optical linewidth of the beam. With this method, the optical linewidth of a single-mode laser can be measured in the electric domain with a RF spectrum analyzer. The implementation of this technique can become quite challenging, as a mode-matching condition must be satisfied. This means that not only must the beams' intensity profiles overlap, but also that their wavefronts must have the same curvature on the detector, so that the interference conditions are uniform over the full detector area. The minimum delay τ_0 required for incoherent mixing must be greater than the inverse of the laser linewidth such that $\tau_0 \geq 1/\Delta\nu$. Figure 3 shows the coherent and incoherent regimes for different fiber optic delay lengths. Longer optical fibers increase the time delay and allow measurement of narrower laser linewidths.
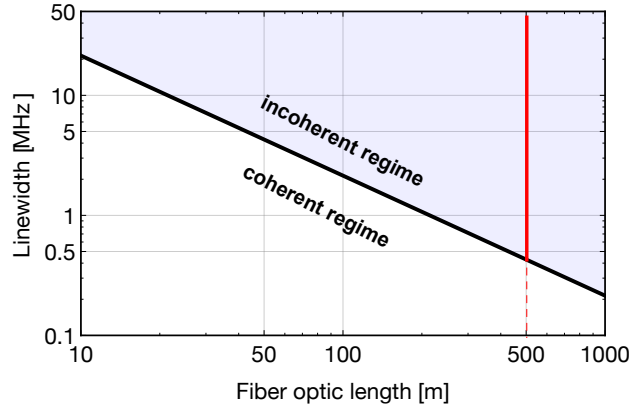

Figure 3. Coherent and incoherent regimes for different fiber optic delay lengths. The shaded region indicates the area where $\tau_0 \geq 1/\Delta\nu$. The red vertical line indicates the coherence regimes for the experiment's fiber optic delay line.

Figure 4 shows the setup for the self-heterodyne linewidth measurements. The AOM is driven with a 107 MHz source, producing a frequency shift in the diffracted orders. The polarization of the zero-order beam is rotated with a half-wave plate and coupled into a polarization-maintaining single-mode optical fiber (PM980-XP) of 500 meters length. The nominal single-mode cut-off wavelength for this fiber is 920 nm, meaning that for shorter wavelengths the fiber is considered multi-mode. The 500 meters optical fiber provides a time delay $\tau_0 = 2.4$ μs,

such that any laser linewidth above 416 kHz is in the incoherent regime, as shown in Figure 3. The two beams are combined in a beamsplitter and coupled into a polarization-maintaining single-mode optical fiber patch cord (PM460-HP) with a cut-off wavelength of 420 nm for mode filtering. The mode-cleaned beam is directly coupled into a fast photodiode (FPD), where the mixing between the two beams takes place. The spectrum of the electrical signal from the photodetector is shown in a spectrum analyzer, where the optical linewidth can be inferred from the electrical power spectrum.
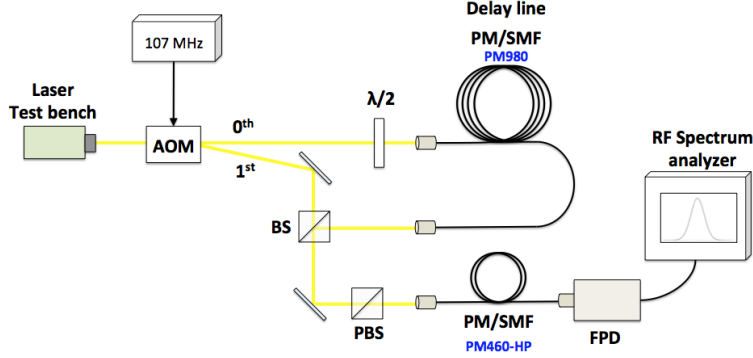

Figure 4. Self-heterodyne linewidth measurements setup.

4. RESULTS

4.1 Laser linewidth

Figure 5 shows the power spectral density from the fast photodiode signal used in the self-heterodyne experiment. For the case of a Lorentzian-shaped laser power spectrum, the displayed lineshape width is twice the linewidth of the laser under test.[13] A Lorentzian fit is applied to the data and the optical linewidth is estimated as half the 3-dB width of the fitted lineshape (FWHM). The linewidth of the 589 nm beam with a Toptica distributed feedback laser seed (DFB) is estimated as 1.34 MHz. The linewidth of the Toptica DLPro laser seed is expected to be much narrower and, indeed, it is expected to be within the coherent regime of our setup (see Figure 3). Our results show that, when using the DLPro seed, different resolution settings of the spectrum analyzer lead to different estimates of the laser linewidth. As shown by Horak,[14] self-heterodyne measurements with a delay line shorter than the coherence time underestimate the actual linewidth. Therefore, our result of 0.02 MHz linewidth should be considered a lower limit. Because we have accurately determined the true linewidth of the Toptica DFB laser, we present the return flux measurements carried out only with this laser seed. Reported measurements of the lifetime for the $3^2P_{3/2}$ state give approximately 16.2 ns.[15] The inverse of the lifetime τ gives the spontaneous decay rate Γ which represents the natural linewidth (as angular frequency) of spontaneous emission. The FWHM natural linewidth of the $3^2P_{3/2}$ state is $\delta\nu = \Gamma/2\pi = 1/(2\pi\tau) = 9.8$ MHz. Because the laser linewidth is smaller than the natural linewidth of sodium, it can only be resonant with one velocity class and it is considered as a single-frequency laser.
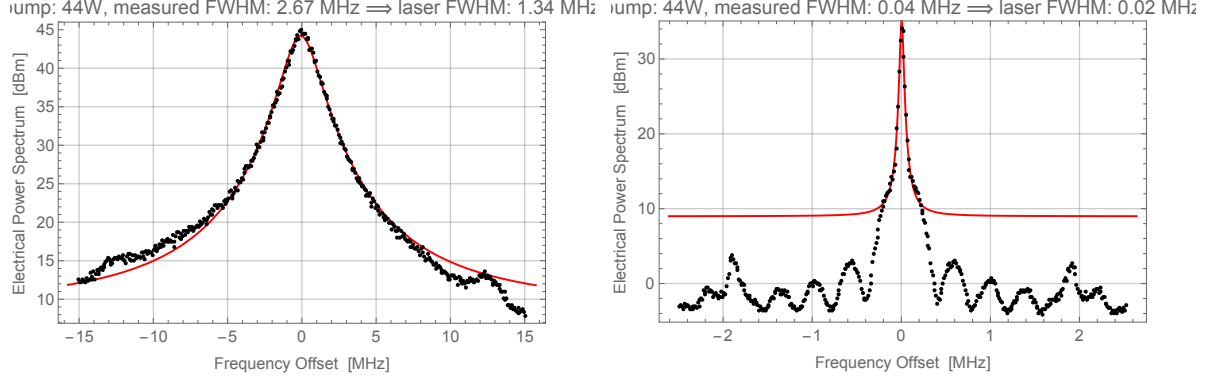
Figure 5. Power spectral density with a Lorentzian fit of the electrical signal from the self-heterodyne linewidth measurement setup, for a Toptica DFB 100 (left) and Toptica DLpro (right) laser seed at 1178 nm. Beat notes are obtained at 589 nm.

4.2 Beam size

Figure 6 shows the x and y axis transverse beam profile obtained with a Thorlabs CCD beam profiler for the apodized beam. Even though the profile is not ideally flat-top it shows substantially higher homogeneity throughout its aperture.

The CCD was positioned at a distance d=185 mm from a focusing lens of 2" aperture and focal length f=250 mm, so the measured beam size must be scaled to obtain the actual beam size at the entrance of the lens according the following relationship:

$$R_0 = R_1 \frac{f}{f-d}, \tag{4}$$

where R_0 is the radius of the collimated beam and R_1 is the measured beam radius at the distance d. In our case, this relationship becomes $R_0 = R_1 \times 3.84$.

The effective beam diameter measured with the CCD is D_{eff}= 5.57 mm, so the effective diameter of the collimated beam is D_0 =21.4 mm. This value is later used to calculate the beam area and the irradiance for a given measured power.
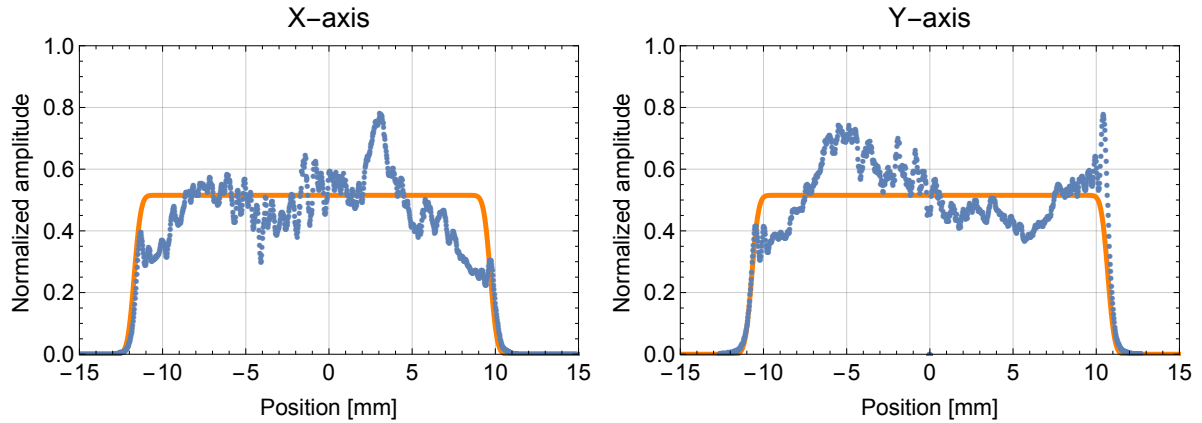

Figure 6. X and Y axis beam profile measurements of the laser focused with a f=250 mm lens into a CCD plane at 185 mm from the input side of the vapor cell. The beam size has been scaled using the equivalence relationships. The effective flat-top profile is plotted for each axis.

4.3 Sidebands

The 1.713 GHz sidebands were generated by using a resonant electro-optic modulator (QUBIG EO-NA23-5K). The EOM generates two sidebands, although only the higher frequency is resonant with the D_2b sodium transition. The "red" sideband (lower frequency) is unused. The repumping power ratio q is:

$$q = \frac{P_{D2b}}{P_{D2a} + P_{D2b}}, \tag{5}$$

where P_{D2a} and P_{D2b} are the power in the D_2a and D_2b transitions respectively.

A sideband power ratio of $q = 10.7\%$ was achieved with 30 dBm of radiofrequency power. Figure 7 shows the spectrum of the laser obtained with a Fabry-Perot spectrum analyzer at the output of the EOM.
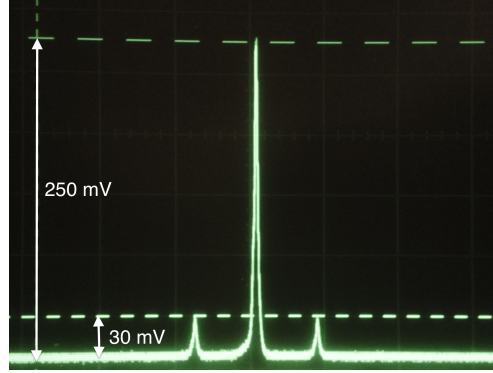

Figure 7. Spectrum of the laser as seen by a Fabry-Perot spectrum analyzer. The sideband power ratio q is 10.7%.

4.4 Fluorescence spectrum

The backward fluorescence spectrum was measured using a narrowband beam of circular polarization and 3.3 W/m^2 intensity scanned in the frequency range of -2 GHz to $+3.5$ GHz with respect to the D_2a resonant frequency. Figure 8 shows the sodium fluorescence spectrum measured in the backward direction. We have simulated the return flux spectrum for two different values of polarization ellipticity: $\widehat{\chi} = 1$ (circular) and $\widehat{\chi} = 0.6$ (elliptical). Although the polarization was set to circular using the waveplates, it is shown that the result assuming an elliptically polarized beam fits better to the measurements. This is a symptom of a systematic polarization impurity that is discussed below. The spectrum also show signs of saturation seen as weak fluorescence on the D_2b transition due to depopulation of the $F = 1$ ground state. Simulations show agreement with observations.
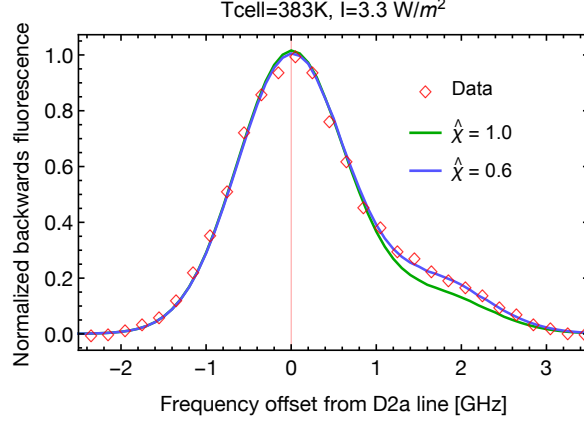
Figure 8. Fluorescence spectrum from a sodium vapor cell and simulated spectrum. The vertical line indicates the center of the sodium D_2 transition. The vapor cell temperature was 383 K and it was illuminated with a flat-top profile beam of circular polarization and intensity 3.3 W/m^2.

4.5 Sodium return flux and simulations

Figure 9 shows the backward fluorescence measurements from a sodium vapor cell for a 1.34 MHz linewidth laser beam resonant with the D_2a sodium transition. The magnetic field angle was oriented 3° with respect to the laser direction with a strength of 0.3 G. The magnetic field strength and direction were measured with a fluxgate magnetometer placed in the center of the oven in the absence of the vapor cell. The data are shown as specific return ψ in units of (photons/s/sr/atom)/(W/m^2). The data are accompanied by a simulation of LGS return flux for a CW narrowband laser and a vapor cell done with the LGSBloch ADM package including all the parameters measured above and specified in Table 1.
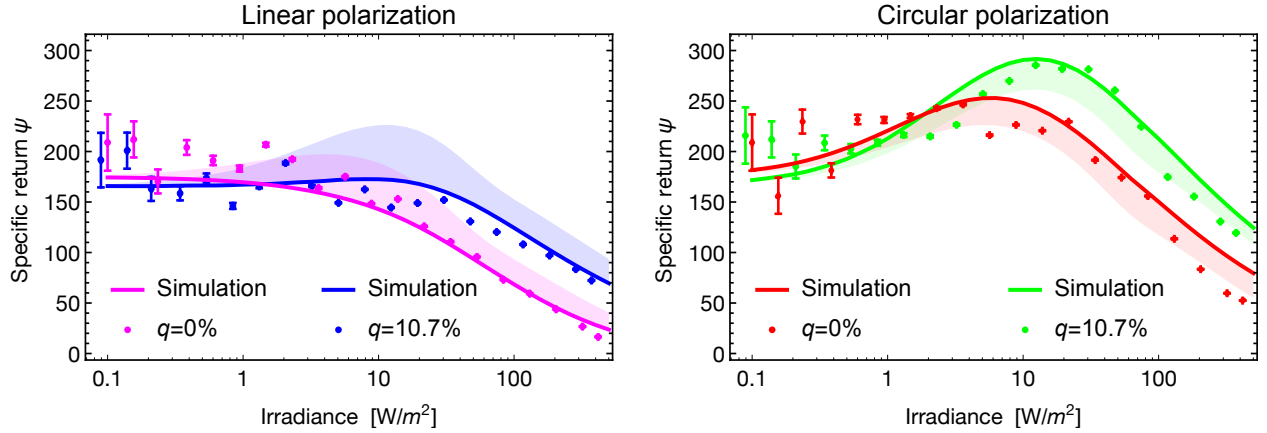

Figure 9. Specific return flux ψ(photons/s/sr/atom/(W/m^2)) obtained with the 1.34 MHz linewidth Toptica DFB seed laser and a sodium vapor cell without buffer gas. Solid lines are pure linear or circular polarization simulations, and shaded regions represent polarization mixing uncertainty. Simulations parameters are shown in Table 1.

The backward fluorescence from the sodium cell is measured with an amplified photodiode, whose analog output is digitized at 100 Hz. Every measurement is the average of 200 acquired samples (two second sample period). Each data point in the plots corresponds to the difference between the backward fluorescence measured on-resonance and off-resonance, and divided by the respective beam intensity. An on-resonance measurement is performed with the laser frequency centered at the D_2a transition, while the off-resonance background measurement is performed with the laser frequency offset by 2 GHz towards lower frequencies.

The statistical error bars given in Figure 9, reflecting effects such as detector noise and laser power noise, show the standard error of the mean $\sigma/\sqrt{N}$ for each collection of samples, where σ is the sample standard deviation and $N = 200$ is the number of samples. Figure 8 shows that for measurements intended to be with circular polarization, the polarization was in fact somewhat elliptical. We have translated this uncertainty into a shaded region around the pure polarization simulations (solid lines). The boundaries are simulations from $\widehat{\chi} = 1$ to $\widehat{\chi} = 0.6$ for circular polarization, and from $\widehat{\chi} = 0$ to $\widehat{\chi} = 0.4$ for linear polarization.

The recorded signal (difference between on-resonance and off-resonance) and the noise for all measurements is shown in Figure 10. The noise (σ) from on-resonance and off-resonance is added in quadrature. The signal becomes small compared to the noise in the low irradiance regime. Increasing noise towards higher irradiance is explained because of larger laser fluctuations. The background (off-resonance) measurements are also shown in Figure 10. The background increases linearly with the intensity but with different slopes for linear or circular polarization. The main sources of background are reflections from the pellicle beamsplitter and from the vapor cell windows, that increase proportional to the input laser power. The different slopes for each polarization are explained by the slightly different polarization splitting ratio of the pellicle beamsplitter used to collect the backward fluorescence. The small difference in the background signal between laser beams with and without repumping is explained by polarization rotation induced by the electro-optic modulator operation.

In all data sets, there is an increasing uncertainty towards lower irradiance values, because the fluorescence signal approaches the noise level reducing the signal-to-background ratio of the measurements. At higher irradiance there are some jumps observed in circular polarization measurements. This might be explained due to polarization rotation due to temperature rising in the EOM crystal.
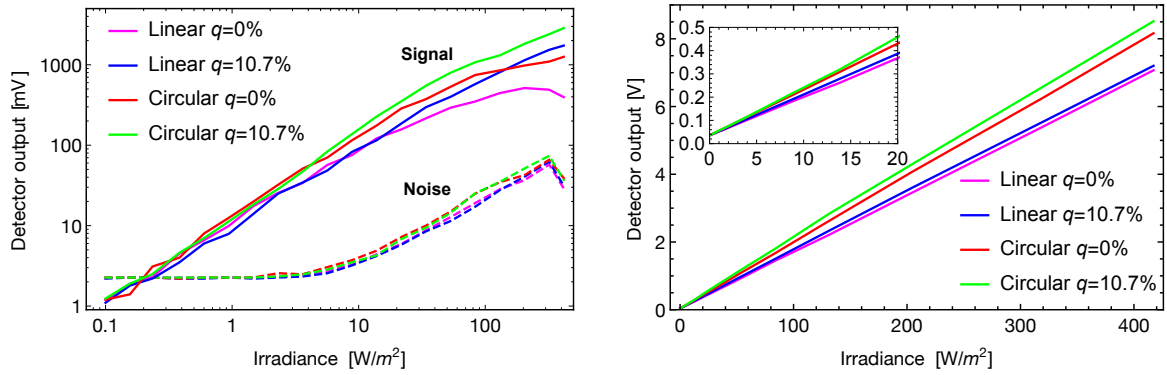

Figure 10. Left: Output voltage from the amplified photodiode for different light intensities. Solid lines show the recorded signal (on-resonance − off-resonance) for each laser polarization and repumping. Dashed lines show the noise recorded for the same intensity scans. Right: Background signal (off-resonance) showing the separation between linear and circular polarization measurements, as well as the splitting when repumping is activated.

Table 1. List of calculated and measured experimental parameters for simulations of vapor cell return flux

Parameter	Nominal value	
Laser wavelength	589.159 nm	
Laser linewidth	1.34 MHz	
Polarization	Linear or circular	
Re-pumping frequency offset	1.713 GHz	
Re-pumping power ratio	0 or 0.107	
Magnetic field	0.3 G	
Magnetic field angle in vapor cell	3°	
	Vapor cell	**Mesosphere**
Beam diameter	21.4 mm	230–1000 mm
Temperature	383 K	170–190 K
Velocity-changing collision rate	Very low	$1/(35~\mu s)$
Spin-exchange collision rate	Very low	$1/(140~\mu s)$
Beam atom exchange rate	$1/(25~\mu s)$	$1/(6.0~ms)$

5. CONCLUSIONS

We have presented a laboratory experiment that allows the comparison of a continuous wave model for return flux of a sodium laser guide star with the backward fluorescence from a sodium vapor cell. We have expressed our results in terms of specific return for direct comparison with the CW sodium LGS model presented by Holzlöhner et al.[10]

The measurements agree with the simulations and show that, with realistic input parameters, the CW LGS model adequately describes the return flux from a vapor-cell. The experiment is mainly affected by low signal-to-noise ratio at low irradiance, and polarization impurities due to the optics chain and the birefringence dependence on temperature of the EOM. Other parameters that introduce a systematic bias along the measurements are the magnetic field angle and strength, and vapor cell temperature, inducing uncertainty in the optical depth of the cell. Despite the seemingly large temperature difference (170 K in the mesosphere vs. 383 K in the cell), the ratio in Doppler broadening and atomic velocities is only $\sqrt{383/170} = 1.5$. Moreover, atomic energy levels do not depend on temperature. Finally, the lack of atom-atom collisions (hence, a large free mean path, no S-damping and no "gentle" velocity-space diffusion with preference to the neighboring velocity classes) in the cell may be regarded as a model of the situation in the upper mesosphere.

We have used a vapor cell filled only with a small amount of sodium. In order to better approximate the conditions of the mesospheric sodium with a vapor cell we will use a vapor cell filled with nitrogen as a buffer gas, yielding velocity-changing collisions and reducing the rate of spin-destruction collisions with the cell wall. Future work involves the introduction of different measurement schemes for return flux and more accurate determination of model input parameters.

ACKNOWLEDGMENTS

REFERENCES

[1] L. A. Thompson and C. S. Gardner, "Experiments on laser guide stars at Mauna Kea Observatory for adaptive imaging in astronomy," *Nature* **328**, pp. 229–231, July 1987.

[2] K. Jin, K. Wei, L. Feng, Y. Bo, J. Zuo, M. Li, H. Fu, X. Dai, Q. Bian, J. Yao, C. Xu, Z. Wang, Q. Peng, X. Xue, X. Cheng, C. Rao, Z. Xu, and Y. Zhang, "Photon return on-sky test of pulsed sodium laser guide star with D2b repumping," *Publications of the Astronomical Society of the Pacific* **127**(954), p. 749, 2015.

[3] H. G. de Chatellus, I. Moldovan, V. Fesquet, and J.-P. Pique, "Suppression of rayleigh scattering noise in sodium laser guide stars by hyperfine depolarization of fluorescence," *Opt. Express* **14**, pp. 11494–11505, Nov 2006.

[4] L. Lihang, H. Wang, W. Hua, Y. Ning, and X. Xu, "Fluorescence enhancing mechanism of optical repumping in sodium atoms for brighter laser guide star," *Opt. Express* **24**, pp. 6976–6984, Apr 2016.

[5] R. Holzlöhner, S. M. Rochester, T. Pfrommer, D. Bonaccini Calia, D. Budker, J. M. Higbie, and W. Hackenberg, "Laser guide star return flux simulations based on observed sodium density profiles," *Proc. SPIE* **7736**, pp. 77360V–77360V–10, 2010.

[6] R. Holzlöhner, D. Bonaccini Calia, D. Budker, M. Centrone, F. Pedreros Bustos, and S. Rochester, "Comparison between observation and simulation of sodium lgs return flux with a 20W CW laser on tenerife," *Proc. SPIE* (9909-178), 2016.

[7] S. Rochester, Atomic Density Matrix package for Mathematica, available online at http://rochesterscientific.com.

[8] P. W. Milonni, H. Fearn, J. M. Telle, and R. Q. Fugate, "Theory of continuous-wave excitation of the sodium beacon," *Journal of the Optical Society of America A* **16**, pp. 2555–2566, Oct. 1999.

[9] J.-P. Pique, I. C. Moldovan, and V. Fesquet, "Concept for polychromatic laser guide stars: one-photon excitation of the 4P3/2 level of a sodium atom," *J. Opt. Soc. Am. A* **23**, pp. 2817–2828, Nov 2006.

[10] R. Holzlöhner, S. M. Rochester, D. Bonaccini Calia, D. Budker, J. M. Higbie, and W. Hackenberg, "Optimization of cw sodium laser guide star efficiency," *AA* **510**, p. A20, Feb. 2010.

[11] P. Atkins, J. de Paula, and R. S. Friedman, *Quanta, Matter and Change: A Molecular Approach to Physical Chemistry*, Oxford Univesity Press., 2009.

[12] M. A. Hafiz, V. Maurice, R. Chutani, N. Passilly, C. Gorecki, S. Gurandel, E. de Clercq, and R. Boudot, "Characterization of cs vapor cell coated with octadecyltrichlorosilane using coherent population trapping spectroscopy," *Journal of Applied Physics* **117**(18), 2015.

[13] D. M. Banet and W. V. Sorin, "Chapter 5: High resolution optical frequency analysis," in *Fiber Optic Test and Measurement*, Hewlet Packard, Prentice Hall, 1998.

[14] P. Horak and W. H. Loh, "On the delayed self-heterodyne interferometric technique for determining the linewidth of fiber lasers," *Opt. Express* **14**, pp. 3923–3928, May 2006.

[15] D. A. Steck, "Sodium D line data." Available online at http://steck.us/alkalidata, revision 2.1.4, 23 December 2010.